A Traction Control System Signal-Based Method for Gear Slack Fault Detection in Electric Locomotive

Qiang Ni, Juntong Liu, Jinxin Zhang, Haohuan Luo, Hanmin Sheng, and Jie Tao

***Abstract*—Gear slack fault (GSF) is a typical fault in traction motor drive system, which will result in the inability to convert motor torque into driving force. However, it is often misdiagnosed as a wheel set idling and speed sensor faults, which can easily cause traction control unit (TCU) to perform incorrect protective actions, leading to safety accidents. Therefore, it is very important to make full use of information collection and calculation capabilities of TCU to detect this fault. In this article, a real-time fault detection method based on time series event mode (TSEM) of multidimensional information in TCU is proposed. First, based on the GSF mechanism, relevant signals are selected, and the feature indexes are extracted. Second, according to the operation condition switching law of the traction system, six TSEMs related to feature indexes are established for representing GSF. Third, the similarity between the real-time sampled window data and each TSEM is calculated. Then, the diagnostic decisions are made by using the obtained similarities. Finally, the proposed real-time fault detection method is verified by the actual operation data. The experimental results show that, comparing with the existing fault detection method, the proposed method has better performance in sensitivity and reliability.**

***Index Terms*—Electric locomotive, fault detection, gear slack fault (GSF), time series event mode (TSEM), traction control unit (TCU), traction motor drive system.**

I. Introduction

ELECTRIC locomotives (ELs) are one of the most important branches of the intelligent transportation. Basically, all ELs are driven by electricity obtained from the catenary through pantograph [1]. As one of the key systems, the electric traction drive system (ETDS) obtains electric power from the pantograph catenary system, converts it into the driving force of traction motor, and then drives the train through the gear drive system [2]. Due to the complex operating environment, the ETDS is susceptible to corrosion, temperature, humidity, power supply surge, static electricity and other factors [3]. Although there is strict regular maintenance based on the mileage, occasional sudden failures are still inevitable during train operation [4]. Therefore, it is of great significance to study real-time and accurate fault detection method to improve system intelligence and to ensure system operation safety [5].

ETDS consists of transformer, rectifier, inverter, dc-link, and motor units. At present, numerous diagnostic and detection methods on typical faults in ETDS have been published. From the diagnostic perspective, they can be divided into two categories, namely, component level and system level. For the component level diagnosis methods, they focus on single or multiple components in ETDS. Representative approaches are a model-based diagnosis method for insulate-gate bipolar transistor (IGBT) open-circuit in three-level rectifier [6], a data-driven diagnostic method for IGBT open-circuit in inverter [7], a model and data hybrid-driven diagnostic method for stator winding interturn short-circuit fault in permanent magnet synchronous motor [8] and a multisensors diagnosis method in traction converters [9]. The above methods only diagnose one fault type, and their diagnosis performance is susceptible to the interference of the associated coupling fault in ETDS. Li et al. [10] and Gou et al. [11] proposed methods for synchronous diagnosis of IGBT and sensors respectively. In fact, the coupling relationship between different components in ETDS is very complex. In addition, component level faults often belong to relatively minor faults, and generally do not trigger ETDS protection in a short time, leading to EL halt.

Regarding system level faults, which are also known as functional faults, refer to the phenomenon of abnormal monitoring signals in the traction control unit (TCU). As compared to component level faults, functional faults are more severe. Once they occur, the EL needs to stop and handle them in a short time to avoid serious accidents. The process of tracking the cause of abnormal phenomenon is diagnosis. Chen et al. [12] proposed a main circuit ground fault diagnosis method for ETDS, Ni et al. [13] improved the diagnostic performance of the main circuit grounding fault. Ni et al. [14] proposed a diagnosis method for grid-side over-current phenomenon in ETDS.

Gear slack fault (GSF) is an abnormal state of gear transmission systems. Once it occurs, traction torque cannot be transmitted to the driven gear and the speed of traction motor of GSF axis will be significantly higher than that of other traction motors, which will cause the idle protection to be activated and

Received 31 August 2024; revised 8 December 2024; accepted 2 February 2025. Date of publication 5 February 2025; date of current version 20 March 2025. This work was supported in part by the National Natural Science Foundation of China under Grant 62103109 and Grant 62373081, in part by the Natural Science Foundation of Guangdong Province under Grant 2024A1515011966, and in part by the Natural Science Foundation of Sichuan Province under Grant 2024NSFSC1483. Recommended for publication by Associate Editor K.-B. Park. *(Corresponding author: Jie Tao.)*

Qiang Ni, Juntong Liu, Jinxin Zhang, Haohuan Luo, and Jie Tao are with the School of Automation, Guangdong University of Technology, Guangzhou 510006, China (e-mail: nq666@gdut.edu.cn; 2112304001@mail2.gdut.edu.cn; 2112404503@mail2.gdut.edu.cn; 3119009375@mail2.gdut.edu.cn; jtao@iipc.zju.edu.cn).

Hanmin Sheng is with the School of Automation, University of Electronic Science and Technology of China, Chengdu 611731, China (e-mail: hmsheng@uestc.edu.cn).

Color versions of one or more figures in this article are available at https://doi.org/10.1109/TPEL.2025.3538789.

Digital Object Identifier 10.1109/TPEL.2025.3538789

the train to be unloaded. If the fault is not diagnosed in a timely manner, the crew will adopt the method of cutting off the idle protection, which can lead to a "sweeping" accident. Therefore, an effective real-time detection of GSF is needed to ensure the train's safety.

Many researchers have published a large number of results on gear fault detection in the electromechanical transmission system [15]. Galloway et al. [16] proposed a representation learning method with three-layer neural network architecture for gear fault diagnosis, which can not only learn bases but also weight bases adaptively. Cheng et al. [17] proposed a deep slow feature analysis and belief-rule-based method for operating gears of high-speed trains. The resampling technology is applied to diagnose the gear faults in [18] by converting the vibration signal into angular domain signal and extracting its envelope and square envelope spectrum features. Wang et al. [19] proposed a convolutional neural network-based gear fault diagnosis method by using variational mode decomposition of the vibration signal. However, although bearing faults have been effectively diagnosed, they are not done from the perspective of improving the performance and safety of the control system using sampled system signals. Furthermore, these methods require vibration information not collected by control system, and diagnostic algorithms cannot be completed in the TCU. The stator current is closely related to the load state of the motor and is an important signal for closed-loop control of the motor. The motor current signal analysis methods are developed to monitor the health condition of gear. Miao et al. [18] investigates the vicinity of the drivetrain frequency of the current spectrum under health and fault conditions. Wang et al. [19] proposed a squeezed modulation signal spectrum method for motor-gear system. Xu et al. [20] and Zhang et al. [21] are only applicable to single motor systems, and their performance in closed-loop control and operating condition change still need further verification. In ETDS, the bogie is composed of three parallel motor transmission shafts. Huang et al. [22] treated all the axles in the bogie as a whole and used the speed information of each axle for slipping detection. Nevertheless, the mechanism of GSF is obviously different from the above applications. Therefore, there is a gap in effectively diagnosing GSF by using the TCU information.

In ETDS, traction motor performs closed-loop control by TCU. The sampled signals and intermediate calculated signals show certain time series changing laws [23]. The time series of stator current, speed and dc-link voltage in induction motor drive systems are learned by extreme learning machine for multisensor fault diagnosis [9]. Chen et al. [24] proposed a hybrid of data and prior knowledge method for IGBT open-circuit fault in rectifier by mining the time series variation law of dc-link voltage, input current and input voltage of pulse rectifier. Shih et al. [9] and Chen et al. [24] are only suitable for situations where the fault duration is long and the fault samples are rich. Ni et al. [14] took the voltage and current from the grid side over-current to the main circuit breaker protection as a time series feature model (TSFM), and traced the causes of the grid side over-current of the traction transformer by identifying the TSFMs. The frequency of voltage and current on the grid side is fixed at 50 Hz. Moreover, the signals in [9], [24], and [14] are all analog signals and sampled by sensors. However, for GSF, to our best knowledge, the related signals include both analog and digital signals, as well as both sampled sensor signals and calculated intermediate signals in the TCU. Furthermore, the speed of the traction motor changes in real-time, it means the frequency of the current is variable. In addition, operating conditions such as traction, braking, and coasting are also dynamically switched. Therefore, how to construct time series event mode (TSEM) is a challenge.

Motivated by the above research gaps, this article will study GSF detection problem from traction control system perspective and propose a TSEM recognition method by fully utilizing the information in TCU and the changes in physical relationships before and after the occurrence of faults. The main contributions of this article can be listed as follows.

1) The GSF detection method is implemented based on signals in TCU without installing additional hardware, rather than the conventional mechanical vibration information or only speed information. The entire bogie is regarded as a whole, and the multiaxis speed signals, traction force signals, and operating condition information in TCU are fully utilized to identify GSF.
2) The problem of GSF detection is transformed into a TSEM recognition problem. Six TSFMs are proposed to represent GSF characteristics by investigating the switching operation condition law. In order to increase the distinguishability of TSFMs, the six templates of TSEM are proposed on the basis of TSFM by studying the changing law of feature indexes under each TSFM.
3) A fault detection method based on similarity comparison between sampling window sequence and time series template is proposed, which improves the sensitivity and robustness of fault detection method and its effectiveness is verified by field experimental data.

The rest of this article is organized as follows. In Section II, the traction motor drive system and mechanism of GSF are introduced. In Section III, feature indexes related to GSF are extracted from system signals, and TSEMs are established. In Section IV, TSEMs and sampling data are quantified as templates and train operating mode, respectively. Then real-time similarity between the operating mode and each template is calculated by DTW algorithm, and GSF is finally judged by CUSUM algorism. In Section V, data from numerous cases are used to verify the effectiveness of the proposed data. Finally, Section VI concludes this article.

II. Traction Motor Drive System and Gear Slack Fault

A. Principle of Torque and Traction Force Conversion

The traction motor dive system in an EL is mainly composed of several basic mechanical units, each of which includes traction motor shaft, axle box, gearbox, and other components as shown in Fig. 1. The traction motor rotor shaft and the driving gear (pinion) are taper fit, and the torque is transmitted through interference connection. During the train operation, TCU controls speed information of traction motors, which are converted into locomotive movement through transmission gear system.

The traction control system collects real-time speed of traction motor rotor shaft from nondrive end (NDE) for closed-loop

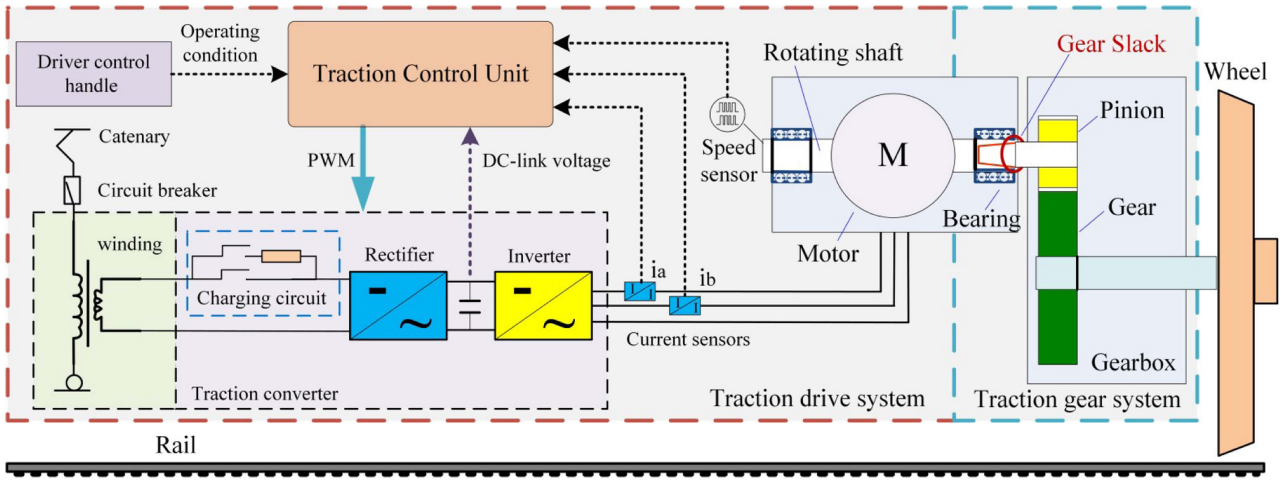

Fig. 1. Traction motor drive system and gear system.

controlling. Normally, the motor rotor shaft and the pinion connecting end are relatively static. The motor traction force F_e is less than the maximum static friction F_s between the motor rotor shaft and the pinion connecting end. The relationship between the rotor shaft speed V_{NDE} and the bogie axle speed V_{BAS} can be expressed as

$$V_{\mathrm{NDE}} = kV_{\mathrm{BAS}} \tag{1}$$

where k is transmission coefficient of the gear. The relationship between traction motor output electromagnetic torque T_e and motor speed V_{NDE} can be written as:

$$T_e - T_L = J\frac{dV_{\mathrm{NDE}}}{dt} + RV_{\mathrm{NDE}} \tag{2}$$

where T_L is the load torque, J represents the moment of inertia, and R denotes the damping coefficient.

B. Mechanism Analysis of Gear Slack Fault

According to analysis of several GSF cases, GSF usually occurs at the joint between the pinion and the motor rotor shaft, or at the sliding point between the motor shaft and the pinion. When it occurs, the motor torque cannot be fully converted into the driving force for the train to move forward. It means that the motor shaft and pinion slip, and the static friction F_s changes into the sliding friction F_r. The T_L, R and J will be greatly reduced and are almost zero, then (2) can be rewritten as

$$\frac{T_e}{J} \approx \frac{dV_{\mathrm{NDE}}}{dt}. \tag{3}$$

Due to TCU performing speed closed-loop control on the fault bogie axle, traction force will be dynamically adjusted so that the V_{NDE} is approximately equal to the given speed. Due to the very small T_L and J on the faulty bogie axle after GSF, a slight amount of traction can cause a rapid change in speed, as shown in Fig. 2. $V_1 \sim V_3$ means the bogie axle speed (V_{BAS}) and a bogie has three axles. $Fe_1 \sim Fe_3$ represents the traction forces of three axes, respectively.

After the traction inverter operates, the operating conditions of the train include traction, braking, and coasting. When the

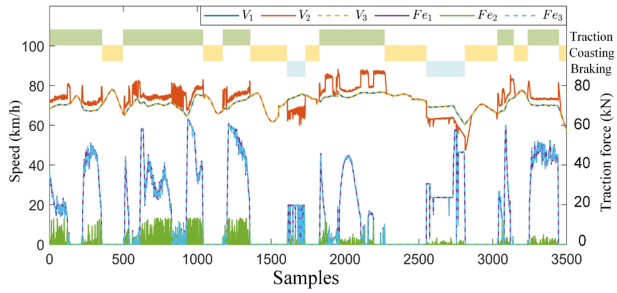

Fig. 2. Related signals of GSF in TCU (the second axis fault).

TABLE I
RELATIONSHIP BETWEEN V_{NDE} AND V_{BAS} UNDER DIFFERENT OPERATING CONDITIONS WHEN GSF OCCURS

Operation conditions	Description of relationship
Traction	$V_{\mathrm{NDE}} > kV_{\mathrm{BAS}}$
Coasting	$V_{\mathrm{NDE}} = kV_{\mathrm{BAS}}$
Braking	$V_{\mathrm{NDE}} < kV_{\mathrm{BAS}}$

GSF occurs, the relationship between V_{NDE} and V_{BAS} can be given in Table I.

III. TIME SERIES FEATURE MODE OF GSF

A. GSF-Related Indexes Extraction

It can be seen from the mechanism of GSF that GSF has a strong correlation with operating condition of EL, V_{NDE}, V_{BAS} and traction force F_e in a bogie. As shown in Fig. 2 and Table I, when a GSF occurs, both the second axle speed and actual traction force show abnormalities, which are strongly related to the operating conditions at that time. The speed of the faulty axle has an abnormal increase in under traction conditions, and due to the dynamic closed-loop regulation of TCU, the actual speed of the faulty axle remains slightly higher than other axles in a dynamic stable state; When under braking conditions, the speed of the faulty axle will be lower than the normal shaft speed through dynamic adjustment of traction force, and the speed difference is uncertain. When under idle working conditions,

TABLE II
RELATED SIGNALS AND FEATURE INDEXES FOR GSF (A BOGIE)

Signals in TCU	Description	Feature indexes	Description
V_{NDE}	Speed of motor rotor	J_1	Operating condition
V_{BAS}	Speed of bogie axles $V_1 \sim V_3$ in Fig.2	J_2	Average speed of axles $(V_1+V_2+V_3)/3$
OC	Operating condition	J_3	Speed of fault axle V_1 or V_2 or V_3
F_e	Traction force	J_4	Average traction force $(Fe_1+Fe_2+Fe_3)/3$
		J_5	Traction force of fault axle Fe_1 or Fe_2 or Fe_3

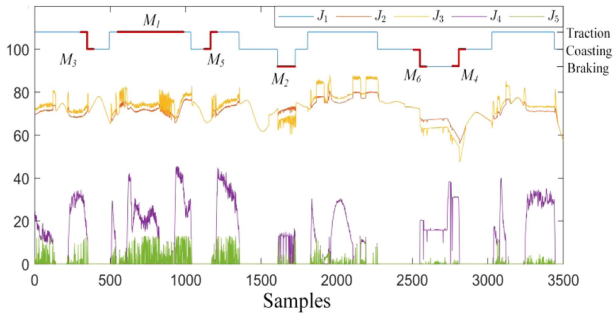

Fig. 3. Feature indexes related signals (the second axis fault).

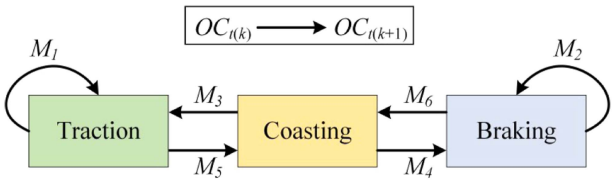

Fig. 4. TSFMs and operating condition (OC) switching modes.

the speed of the faulty axle is equal to the normal axle speed. Therefore, this article selects these three types of information to extract faulty indexes. As shown in Fig. 1, an EL usually has two bogies, each of which has three bogie axles. Normally, the traction force and speed of each bogie axle are equal. Therefore, feature indexes are extracted for representing GSF, as given in Table II.

Based on historical data, the variation law of feature indexes $J_1 - J_5$ can be obtained, as shown in Fig. 3.

B. Forming TSFMs With Extracted Indexes

In actual operation, EL has three operation conditions, that is, traction, coasting, and braking. As shown in Figs. 2 and 3, during EL operation, the operation conditions are dynamically switched and the dynamic process only has a short duration. Therefore, in this article, this dynamic process is described by using five consecutive sampling points. Based on engineering knowledge and data analysis, there are a total of six operation condition switching modes, as shown in Fig. 4. The GSF characteristics in each mode can be described by the time series matrix of feature

TABLE III
CHANGING CHARACTERISTICS OF FEATURE INDICATORS IN EACH TSFM

TSFM	Description
M_1	J_1: Traction, $J_2 - J_3 < 0$, $J_4 - J_5 > 0$;
M_2	J_1: Braking, $(J_2 - J_3 > 0)$, $(J_4 - J_5 > 0)$;
M_3	J_1: From traction to braking; From $(J_2 - J_3 < 0)$ to $(J_2 - J_3 \approx 0)$; From $(J_4 - J_5 > 0)$ to $(J_4 - J_5 \approx 0)$;
M_4	J_1: From braking to coasting; From $(J_2 > J_3)$ to $(J_2 - J_3 \approx 0)$; From $(J_4 > J_5)$ to $(J_4 \approx J_5 \approx 0)$;
M_5	J_1: Coasting to traction, $(J_2 - J_3 \approx 0)$ to $(J_2 - J_3 < 0)$, $(J_4 - J_5 \approx 0)$ to $(J_4 - J_5 > 0)$;
M_6	J_1: From coasting to braking; from $(J_2 - J_3 \approx 0)$ to $(J_2 > J_3)$, from $(J_4 - J_5 \approx 0)$ to $(J_4 - J_5 > 0)$;

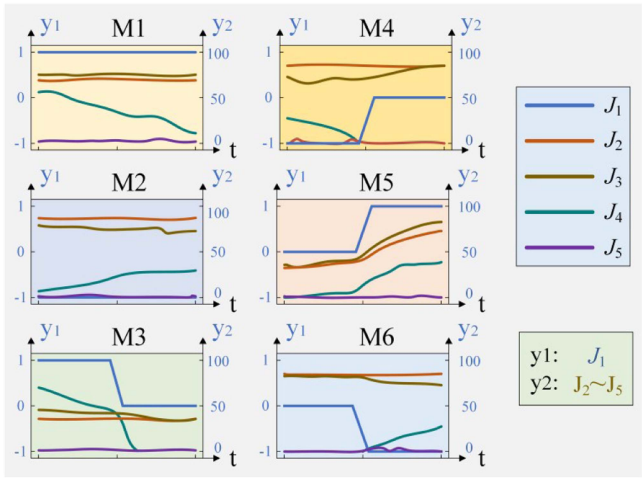

Fig. 5. Feature indexes of time series in different TSFMs.

indexes. Six TSFMs can be written as

$$M_i = \begin{bmatrix} J_1(k-4) & \cdots & J_1(k-1) & J_1(k) \\ J_2(k-4) & \cdots & J_2(k-1) & J_2(k) \\ \vdots & \cdots & \vdots \cdots & \vdots \\ J_5(k-4) & \cdots & J_5(k-1) & J_5(k) \end{bmatrix} \quad (4)$$

where i represents an integer between 1 and 6, k represents the current sampling time, and M_i means ith TSFM.

The changing rules of feature indexes in each TSFM are given in Table III.

IV. REAL-TIME GSF DETECTION BASED ON SIMILARITY COMPARISON

It can be seen from Fig. 5 and Table III that GSF can be represented by TSFMs. Therefore, if the sampling data is sufficiently similar to one of them, the axle of the sampling source is diagnosed as GSF. However, when two series with different data lengths are compared, the result based on conventional distance calculation methods (such as Euclidean distance) will have a large deviation from the actual result. Besides, the result is ineffective if the similarity between the analog sampling data and TSFMs are directly compared without quantification.

In this section, to tackle the above problems, we first quantify the TSFMs to TSEMs and the sampling data as fault templates

TABLE IV
TEMPLATES OF TSEM AFTER DISCRETIZATION

Mode	$\tilde{J}_1$	$\tilde{J}_2$	$\tilde{J}_3$	$\tilde{J}_4$	$\tilde{J}_5$
$\tilde{M}_1$	(11111)	(00000)	(11111)	(11111)	(00000)
$\tilde{M}_2$	(-1-1-1-1-1)	(11111)	(00000)	(11111)	(00000)
$\tilde{M}_3$	(11100)	(00000)	(11100)	(11100)	(00000)
$\tilde{M}_4$	(-1-1-100)	(11100)	(00000)	(11100)	(00000)
$\tilde{M}_5$	(00011)	(00000)	(00011)	(00011)	(00000)
$\tilde{M}_6$	(000-1-1)	(00011)	(00000)	(00011)	(00000)

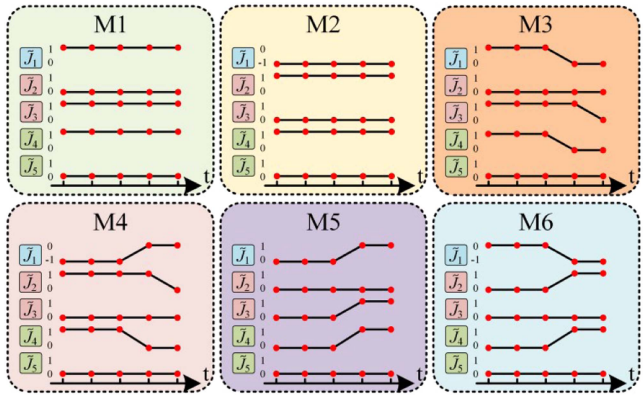

Fig. 6. Fault templates established by quantifying TSEMs.

and current train operating mode, and then use DTW algorithm to calculate the similarity in between. Finally, GSF is diagnosed by using CUSUM algorithm.

A. TSFMs and Sampling Data Quantification

As shown in Figs. 3 and 5, the feature indicators under the six modes have obvious temporal variation patterns. J_1 reflects changes in operating conditions, with only three states and not continuous variables, exhibiting distinct event characteristics. As shown in Fig. 5 and Table III, the J_3 and J_2 describe the variation pattern of speed information between the fault axis and the overall axis, the J_5 and J_4 describe the variation pattern of traction force information between the fault axis and the overall axis. The difference between J_1 and J_2, as well as the difference between J_3 and J_4, exhibit hysteresis switching characteristics in different TSFM. Therefore, the feature indexes can be discretized into events for increasing the distinguishability of TSFMs, and then the TSFM will be converted to TSEM.

The feature index J_1 that represents the operating conditions of the train is quantified as

$$\tilde{J}_1 = \begin{cases} 1, & J_1 = DR \\ -1, & J_1 = BR \\ 0, & J_1 = ZO \end{cases}. \tag{5}$$

Feature indexes $J_2 - J_3$ and $J_4 - J_5$ that respectively represent traction force and speed information are quantified as

$$\begin{cases} \tilde{J}_2 = 1,\ \tilde{J}_3 = 0, & J_2 - J_3 > E_V \\ \tilde{J}_2 = 0,\ \tilde{J}_3 = 0, & |J_2 - J_3| > E_V \\ \tilde{J}_2 = 0,\ \tilde{J}_3 = 1, & J_2 - J_3 < -E_V \end{cases} \tag{6}$$

$$\begin{cases} \tilde{J}_4 = 1,\ \tilde{J}_5 = 0, & J_4 - J_5 > E_{\mathrm{Fe}} \\ \tilde{J}_4 = 0,\ \tilde{J}_5 = 0, & |J_4 - J_5| > E_{\mathrm{Fe}} \\ \tilde{J}_4 = 0,\ \tilde{J}_5 = 1, & J_4 - J_5 < -E_{\mathrm{Fe}} \end{cases} \tag{7}$$

where E_V represents the threshold of speed difference among axles, E_{Fe} represents the threshold of traction force difference among axles. After the discretization, templates of TSEM are established (see Fig. 6 and Table IV). In this article, lengths of template are all set to 5.

According to the GSF-relevant signals captured from the data sampling window, TCU continuously extracts feature indexes $J_1 - J_5$ and saves as time series $\boldsymbol{J}_1 - \boldsymbol{J}_5$, which are quantified to obtain the train operating mode of the sampling data at current time k. It is written as

$$\begin{bmatrix} \tilde{\boldsymbol{J}}_1(k,N) \\ \tilde{\boldsymbol{J}}_2(k,N) \\ \vdots \\ \tilde{\boldsymbol{J}}_5(k,N) \end{bmatrix} = \begin{bmatrix} \tilde{J}_1(k-N+1) & \tilde{J}_1(k-N+2) & \cdots & \tilde{J}_1(k) \\ \tilde{J}_2(k-N+1) & \tilde{J}_2(k-N+2) & \cdots & \tilde{J}_2(k) \\ \vdots & \vdots & \ddots & \vdots \\ \tilde{J}_5(k-N+1) & \tilde{J}_5(k-N+2) & \cdots & \tilde{J}_5(k) \end{bmatrix} \tag{8}$$

where $\tilde{\boldsymbol{J}}_1(k,\ N) - \tilde{\boldsymbol{J}}_5(k,\ N)$ represent quantified feature indexes of time series, N is the number of samples included in the series which is set to 10 in this article.

B. Fundamental Principal of DTW Algorithm

DTW algorithm, which solves the problem of time scale synchronization, is commonly used in measuring the similarity between two given series with different lengths [23]. It combines time warping and distance measuring to calculate the optimal match of two series.

Suppose two time series $S = \{s_1, s_2, \ldots, s_n\}$ and $Q = \{q_1, q_2, \ldots, q_m\}$, and a matrix $D_{\mathrm{n\times m}}$ is defined as

$$D(i,j) = ||s_i - q_j||_w \tag{9}$$

where position (i, j) of the matrix contains the alignment cost between s_i and q_j $(i = 1, 2, \ldots, n;\ j = 1, 2, \ldots, m;\ w = 2)$.

Suppose that $p_1 - p_{\mathrm{L}}$ are points along the warping path, the restrictions of DTW are listed as follows.

1) Boundary conditions: $p_1 = (1, 1)$ and $p_L = (n, m)$.
2) Monotonicity: Each point on the path must monotonously change with time, which can be described as $n_1 \le n_i \le n_L$, $m_1 \le m_i \le m_L$.
3) Continuity: For a point $p_{\mathrm{i}} = (s_{\mathrm{i}}, q_{\mathrm{i}})$ and the following point $p_{i+1} = (s_{i+1}, q_{i+1})$ on the path, $s_{i+1} - s_i \le 1$ and $q_{i+1} - q_i \le 1$.

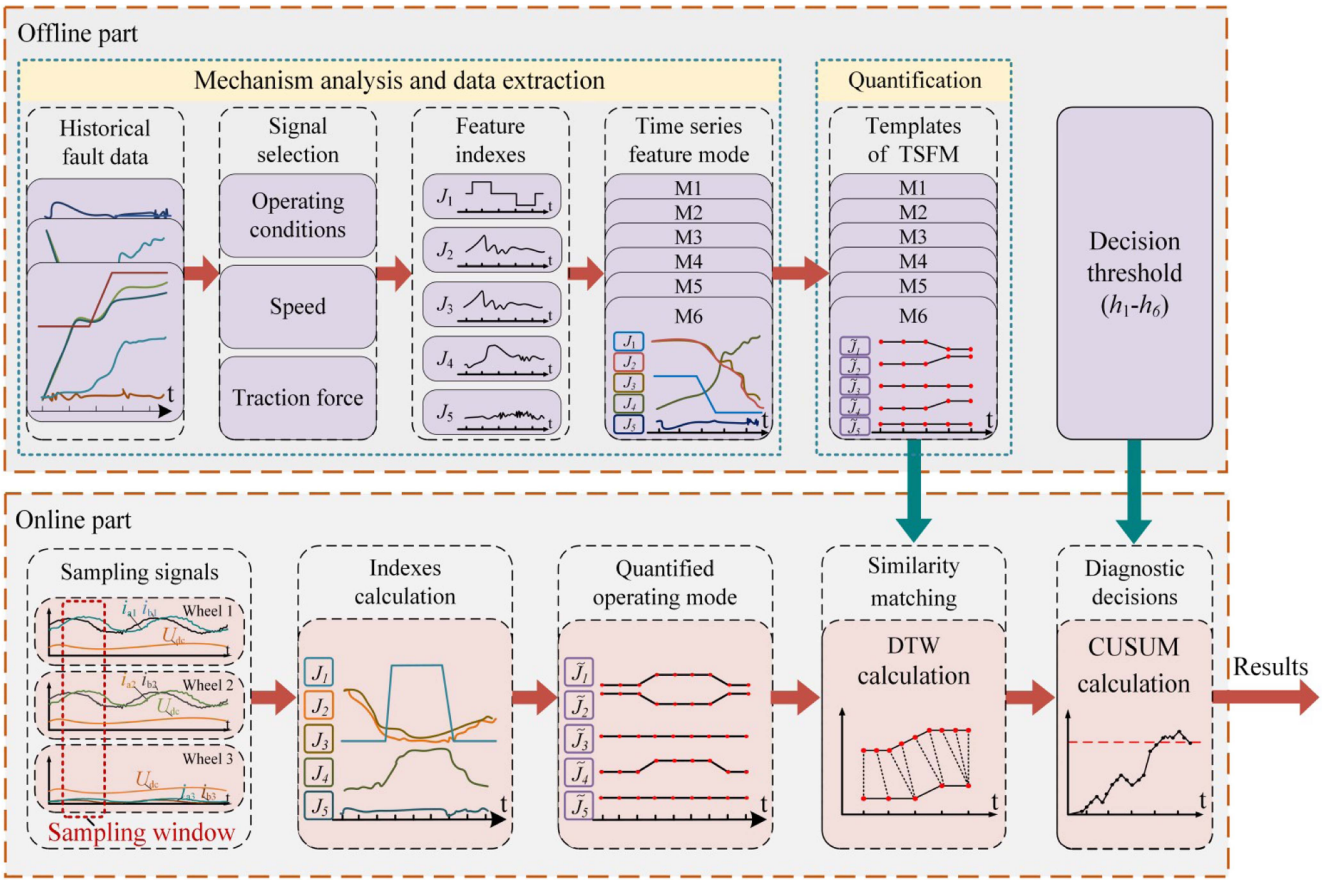

Fig. 7. Flow chart of the proposed real-time fault detection method.

All of the warping paths between the time series S and Q are calculated according to the formula $d(x_n, y_m) = (x_n, y_m)^2$. Then the optimal path $P = (p_1, p_2, \ldots, p_k)$ are found so that the cumulative distance $d(n, m)$ is the minimum. It is written as

$$\mathrm{DTW}(S, Q) = \min\left(\sum_{k=1}^{K} p_k\right) = d(n, m) \tag{10}$$

where the cumulative distance is

$$d(i, j) = D(i, j) + \min\begin{cases}\gamma(i-1, j-1)\\ \gamma(i-1, j)\\ \gamma(i, j-1)\end{cases}. \tag{11}$$

C. Similarity Calculation

Similarity function $d_{ij}(k)$ are defined as shown in (12), and (13) is defined to find out the maximum similarity between the operating mode and TSFM templates at the current time k

$$d_{ij}(k) = f_{\mathrm{DTW}}\left(\tilde{\boldsymbol{J}}_i(k, N), \boldsymbol{M}_j^{(i)}\right) \tag{12}$$

$$s_j(k) = \max\left(d_{1j}(k), d_{2j}(k), \cdots, d_{5j}(k),\right) \tag{13}$$

where f_{DTW} is an operator of DTW algorithm, $\tilde{\boldsymbol{J}}_i(k, N)$ represents the ith quantified feature index of time series with samples of N at the current time k in the sampling window, $\boldsymbol{M}_j^{(i)}$ represents the ith time series feature index of the jth template of TSFM.

D. GSF Detection Decision-Making

Considering the existence of a certain degree of noise and interference in sampling signals, and in order to improve the reliability of GSF detection, GSF is finally diagnosed by using CUSUM algorithm [24]. Defining the decision-making function as

$$g_j(k) = \max\left(0, g_j(k-1) + TS_j - s_j(k)\right) \tag{14}$$

where TS_j is the similarity threshold between two compared series. The following fault decision logic is adopted as

$$F_j(k) = \begin{cases}1, & g_j(k) > h_j\\ 0, & g_j(k) \le h_j\end{cases} \tag{15}$$

$$F(k) = \begin{cases}1, & \exists F_j(k) = 1\\ 0 & \forall F_j(k) = 0\end{cases} \tag{16}$$

where $h_j\ (j = 1, 2, \ldots, 6)$ represents the fault-diagnosed threshold, which can be set based on application experience, $F_j\ (j = 1, 2, \ldots, 6)$ is the sub flag of GSF, and $F_j = 1$ represents the fault occurrence related to the jth template; F is the general flag of GSF, and 1 represents GSF occurrence. The whole process of GSF real-time detection is shown in Fig. 7.

Fig. 8. HXD1C electric locomotive.

V. Field Experiment and Results

A. Data Description

To verify the effectiveness of the proposed fault detection method, this section conducts experiment based on field data collected from the HXD1C EL equipped with six axles (see Fig. 8). TCU collects signals from sensors and executive parts in the traction drive system. As a module in TCU, the subprogram of GSF detection captures information, including traction force and speed of each axle, and operating conditions of the train from the TCU buffer and recording waves as a fault case. Each case has a total of 15 000 points, including information before and after the fault and the sampling period is 0.3 s. The total number of collected sample cases include normal data case, real relaxation faults case, speed sensor malfunction case and wheelset idle case.

The experiment consists of two parts. The first part verifies the advantages of the proposed method compared with the existing engineering (EE) method based on GSF case data. The second part verifies the robustness of the proposed method by using speed sensor fault case data and wheel set idling fault case data. In this experiment, the data window N of feature indexes calculation is set to 10, because the length of each template is all set to 5 and it is enough to contain template information.

B. Performance Indicator

To objectively show the advantages of the proposed method, fault detection rate (FDR) is introduced as the performance indicator [13], which is used to illustrate the detection sensitivity. The calculation form of FDR is given as follows:

$$\mathrm{FDR} = \frac{\mathrm{Num}(f_{\mathrm{detect}}|f_{\mathrm{real}})}{N_f} \times 100\% \tag{17}$$

where N_f is total fault samples, f_{real} denotes the real happened fault, f_{detect} denotes the detected fault, and $\mathrm{Num}(f_{\mathrm{detect}}|f_{\mathrm{real}})$ represents the number of faults detected in case of all GSF.

C. Results Analysis

In tests of the EE method, when the speed of the tested axle exceeds the threshold V_{MAXth} or the difference amount each axle exceeds the threshold ΔV_{th}, the EE method determines the occurrence of the GSF. The process of detection can be written as

$$F = 1 \quad \forall (V_i > V_{\mathrm{MAXth}},\ V_i - V_{\mathrm{aver}} > \Delta V_{\mathrm{th}}) \tag{18}$$

where F is initially set to 0, V_i denotes the speed of the tested axle, V_{aver} denotes the average speed of the tested frame. V_{MAXth} is set to 140 km/h and ΔV_{th} is set to 5 km/h in this experiment.

In the first part of the experiment, the advanced performance of the proposed method is demonstrated by comparing with the EE method in a GSF case. As shown in Fig. 9, GSF occurs on the fifth axle. It can be seen from Fig. 9(a)–(c) that the fault axle appears no difference to normal axles when the system is working in idling condition. When operating condition switches to traction, the speed of the fault axle shows an abnormal rise and then consistently keeps a slightly higher value compared to the normal ones, and the traction force fluctuates around 0. In the starting stage of the fault, due to the closed-loop speed control, the speed difference between the fault and the normal axles is too small to detect by using the EE method. As the

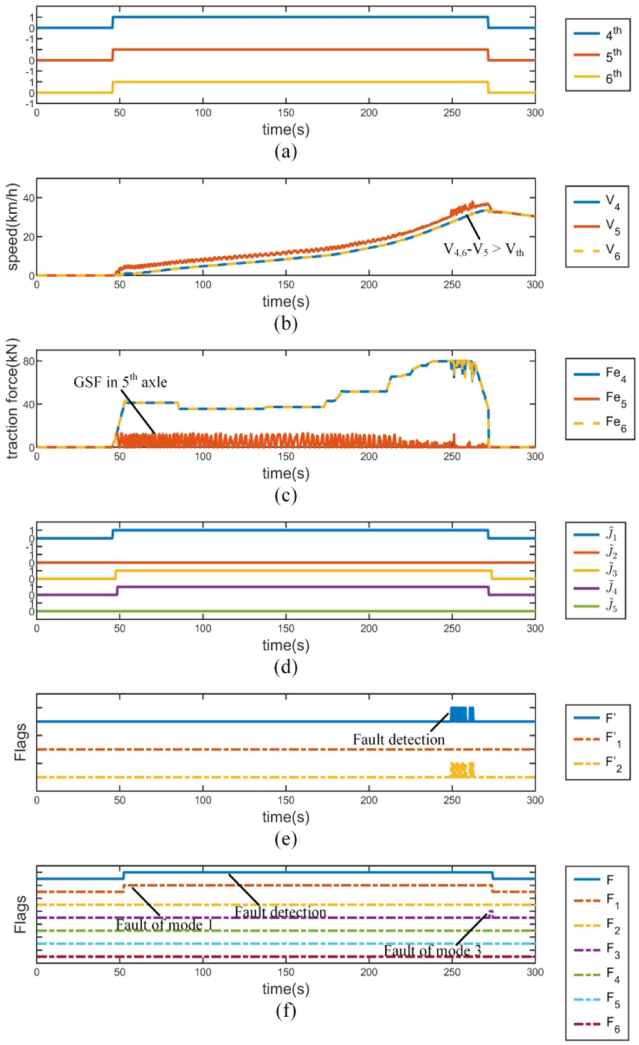

Fig. 9. Real gear slack fault case. (a) Operating condition of the train. (b) Train speed Variation. (c) Traction force Variation. (d) Quantified GSF-relevant feature indexes. (e) Fault flags of the EE method. (f) Fault flags of the proposed method.

TABLE V
PERFORMANCE COMPARISON

Index	Case 1	Case 2
Time point of fault	46.7s	145.5s
Fault detection point (DTW)	53.2s	171.9s
Fault detection point (EE)	248.5s	372.3s
FDR (Proposed)	97.34%	98.66%
FDR (EE)	7.11%	2.94%

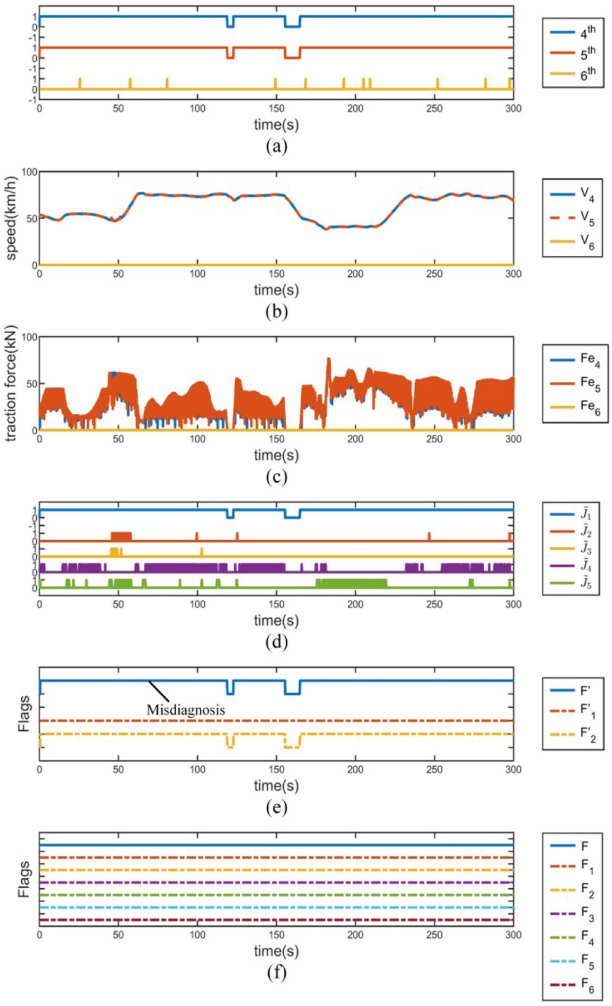

Fig. 10. Speed sensor fault case. (a) Operating condition of the train. (b) Train speed Variation. (c) Traction force Variation. (d) Quantified GSF-relevant feature indexes. (e) Fault flags of the EE method. (f) Fault flags of the proposed method.

degree of fault increases, the fault will not be detected until the speed difference exceeds the limit. However, this type of fault can be easily discovered by the proposed method. It can be seen from Fig. 9(d)–(f) that relevant feature indexes of time series can describe GSF in detail, and diagnoses it as fault of mode 1 within 4 s. In addition, in order to prove the universality of the proposed method, comparisons of performance in different cases are given in Table V.

To further verify the effectiveness of the proposed method, the robustness experiments are performed under two interference cases. Fig. 10 shows the results of the experiment with

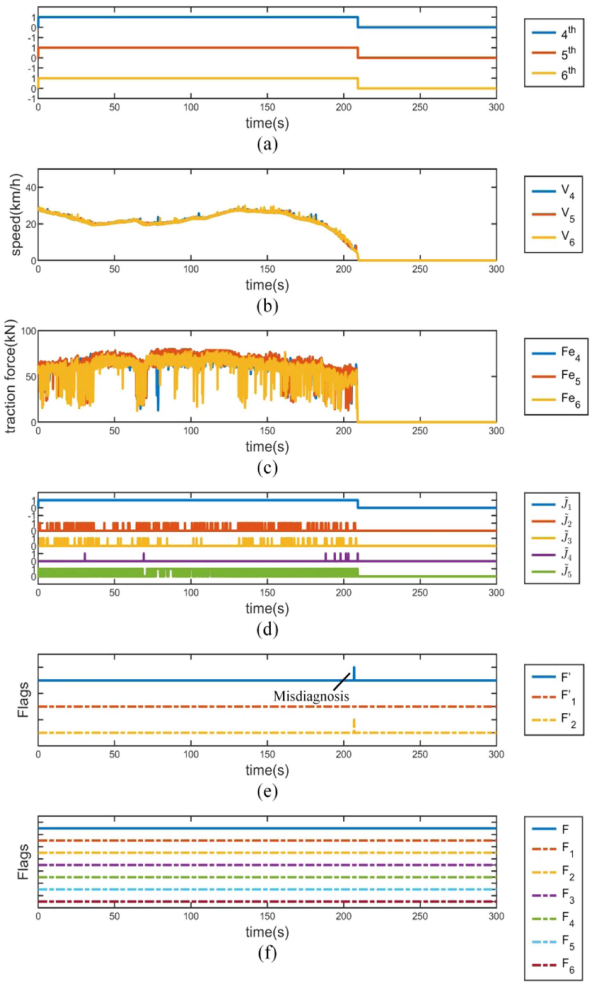

Fig. 11. Wheel set idling case. (a) Operating condition of the train. (b) Train speed Variation. (c) Traction force Variation. (d) Quantified GSF-relevant feature indexes. (e) Fault flags of the EE method. (f) Fault flags of the proposed method.

unavailable sixth speed sensor. It can be seen from Fig. 10(b) that the speed of the sixth axle measured by the fault sensor remains in zero value, which means that the speed difference between axles excess the threshold ΔV_{th}. As a result, TCU isolates the fault axle traction from the system and misdiagnoses the fault as GSF by using the EE method. In contrast, the operating mode does not match any of the template modes when using the proposed method.

Fig. 11 shows an experiment conducted under wheel set idling condition. It can be seen from Fig. 11(b) that at the point around 210 s, the traction force plunges to 0, which denotes that the power of the shaft cannot be transmitted to the fault wheel set. After losing the traction, the speed of the train steadily decreases until the train stops. The same mechanism as the last experiment, the EE method misdiagnoses the fault while the proposed method is robust enough to diagnose the fault is irrelevant to GSF.

It is obvious that compared to the existing detection method, the proposed method can detect the GSF in an early stage, and seldomly misdiagnose it. In other words, the proposed detection method has better performance in sensitivity and robustness.

VI. Conclusion

This article addressed the problem of GSF detection from the perspective of monitoring signals from traction control systems, which differs from the conventional method based on mechanical vibration signal. A time series event mode recognition-based method for GSF detection is proposed based on signals in TCU without additional hardware. The fault TSFMs are proposed by combining knowledge of switching operation conditions and data analysis. Based on the characteristics of feature index, the TSFMs are converted into TSEMs. The GSF is diagnosed in real-time by measuring the similarity between the sampled window data and the templates of TSEM.

The proposed method is applied to a real-life electrical traction system and is verified by using actual field test data. The experimental results show that the proposed approach is superior to the conventional one with respect to FDR and detection delay in case of GSF. Furthermore, the proposed method has strong robustness in case of the speed sensor fault and wheel set idling cases. According to the obtained results, it can be seen that the proposed method with its simpler form and lower design efforts is promising for GSF detection.

References

[1] X. Meng, Z. Liu, G. Li, X. Chen, S. Wu, and K. Hu, "A multi-frequency input-admittance model of locomotive rectifier considering PWM sideband harmonic coupling in electrical railways," *IEEE Trans. Transp. Electrific.*, vol. 8, no. 3, pp. 3848–3858, Sep. 2022.

[2] H. Tao, H. Hu, X. Zhu, K. Lei, and Z. He, "A multifrequency model of electric locomotive for high-frequency instability assessment," *IEEE Trans. Transp. Electrific.*, vol. 6, no. 1, pp. 241–256, Mar. 2020.

[3] H. Chen and B. Jiang, "A review of fault detection and diagnosis for the traction system in high-speed trains," *IEEE Trans. Intell. Transp. Syst.*, vol. 21, no. 2, pp. 450–465, Feb. 2020.

[4] Y. Zhang, N. Qin, D. Huang, and J. Du, "Precise diagnosis of unknown fault of high-speed train bogie using novel FBM-Net," *IEEE Trans. Instrum. Meas.*, vol. 71, 2022, Art. no. 3526811.

[5] G. Yang, H. Hussain, S. Li, J. Zhang, and J. Yang, "Fault-tolerant control for multiphase induction machines with torque ripple reduction considering harmonic injection," *IEEE Trans. Power Electron.*, vol. 37, no. 12, pp. 14005–14010, Dec. 2022.

[6] C. Yang, W. Gui, Z. Wen, J. Zhang, T. Peng, and C. Yang, "Voltage difference residual-based open-circuit fault diagnosis approach for three-level converters in electric traction systems," *IEEE Trans. Power Electron.*, vol. 35, no. 3, pp. 3012–3028, Mar. 2020.

[7] Y. Xia, Y. Xu, and B. Gou, "A data-driven method for IGBT open-circuit fault diagnosis based on hybrid ensemble learning and sliding-window classification," *IEEE Trans. Ind. Inform.*, vol. 16, no. 8, pp. 5223–5233, Aug. 2020.

[8] B. Gou, Y. Xu, Y. Xia, G. Wilson, and S. Liu, "An intelligent time-adaptive data-driven method for sensor fault diagnosis in induction motor drive system," *IEEE Trans. Ind. Electron.*, vol. 66, no. 12, pp. 9817–9827, Dec. 2019.

[9] K.-J. Shih, M.-F. Hsieh, B.-J. Chen, and S.-F. Huang, "Machine learning for inter-turn short-circuit fault diagnosis in permanent magnet synchronous motors," *IEEE Trans. Magn.*, vol. 58, no. 8, Aug. 2022, Art. no. 8204307.

[10] X. Li, J. Xu, Z. Chen, S. Xu, and K. Liu, "Real-time fault diagnosis of pulse rectifier in traction system based on structural model," *IEEE Trans. Intell. Transp. Syst.*, vol. 23, no. 3, pp. 2130–2143, Mar. 2022.

[11] B. Gou, Y. Xu, Y. Xia, Q. Deng, and X. Ge, "An online data-driven method for simultaneous diagnosis of IGBT and current sensor fault of three-phase PWM inverter in induction motor drives," *IEEE Trans. Power Electron.*, vol. 35, no. 12, pp. 13281–13294, Dec. 2020.

[12] Z. Chen et al., "A data-driven ground fault detection and isolation method for main circuit in railway electrical traction system," *ISA Trans.*, vol. 87, pp. 264–271, Dec. 2019.

[13] Q. Ni, Z. Zhan, X. Li, Z. Zhao, and L. L. Lai, "A real-time fault diagnosis method for grid-side overcurrent in train traction system using signal time series feature pattern recognition," *IEEE Trans. Ind. Electron.*, vol. 71, no. 4, pp. 4210–4218, Apr. 2024.

[14] Q. Ni, X. Li, Z. Chen, Z. Zhao, and L. L. Lai, "A mechanism and data hybrid-driven method for main circuit ground fault diagnosis in electrical traction system," *IEEE Trans. Ind. Electron.*, vol. 70, no. 12, pp. 12806–12815, Dec. 2023.

[15] Y. Wang, B. Tang, Y. Qin, and T. Huang, "Rolling bearing fault detection of civil aircraft engine based on adaptive estimation of instantaneous angular speed," *IEEE Trans. Ind. Inform.*, vol. 16, no. 7, pp. 4938–4948, Jul. 2020.

[16] G. S. Galloway, V. M. Catterson, C. Love, A. Robb, and T. Fay, "Modeling and interpretation of tidal turbine vibration through weighted least squares regression," *IEEE Trans. Syst., Man, Cybern.: Syst.*, vol. 50, no. 4, pp. 1252–1259, Apr. 2020.

[17] C. Cheng, X. Qiao, H. Luo, G. Wang, W. Teng, and B. Zhang, "Data-driven incipient fault detection and diagnosis for the running gear in high-speed trains," *IEEE Trans. Veh. Technol.*, vol. 69, no. 9, pp. 9566–9576, Sep. 2020.

[18] J. Miao, J. Wang, and Q. Miao, "An enhanced multifeature fusion method for rotating component fault diagnosis in different working conditions," *IEEE Trans. Rel.*, vol. 70, no. 4, pp. 1611–1620, Dec. 2021.

[19] M. Wang, X. Ma, Y. Hu, and Y. Wang, "Gear fault diagnosis based on variational modal decomposition and wide+narrow visual field neural networks," *IEEE Trans. Automat. Sci. Eng.*, vol. 19, no. 4, pp. 3288–3299, Oct. 2022.

[20] Y. Xu, X. Tang, X. Sun, F. Gu, and A. D. Ball, "A squeezed modulation signal bispectrum method for motor current signals based gear fault diagnosis," *IEEE Trans. Instrum. Meas.*, vol. 71, 2022, Art. no. 3521508.

[21] J. Zhang, J. S. Dhupia, and C. J. Gajanayake, "Stator current analysis from electrical machines using resonance residual technique to detect faults in planetary gearboxes," *IEEE Trans. Ind. Electron.*, vol. 62, no. 9, pp. 5709–5721, Sep. 2015.

[22] J. Huang, B. Jiang, C. Xu, and N. Wang, "Slipping detection of electric locomotive based on empirical wavelet transform, fuzzy entropy algorithm and support vector machine," *IEEE Trans. Veh. Technol.*, vol. 70, no. 8, pp. 7558–7570, Aug. 2021.

[23] H. Chen, B. Jiang, S. X. Ding, and B. Huang, "Data-driven fault diagnosis for traction systems in high-speed trains: A survey, challenges, and perspectives," *IEEE Trans. Intell. Transp. Syst.*, vol. 23, no. 3, pp. 1700–1716, Mar. 2022.

[24] Z. Chen, J. Xu, T. Peng, and C. Yang, "Graph convolutional network-based method for fault diagnosis using a hybrid of measurement and prior knowledge," *IEEE Trans. Cybern.*, vol. 52, no. 9, pp. 9157–9169, Sep. 2022.

[25] Z. Zheng et al., "A fused method of machine learning and dynamic time warping for road anomalies detection," *IEEE Trans. Intell. Transp. Syst.*, vol. 23, no. 2, pp. 827–839, Feb. 2022.

[26] K.-D. Lu and Z.-G. Wu, "Genetic algorithm-based cumulative sum method for jamming attack detection of cyber-physical power systems," *IEEE Trans. Instrum. Meas.*, vol. 71, 2022, Art. no. 9004810.

Qiang Ni received the M.S. and Ph.D. degrees in electrical engineering from Southwest Jiaotong University, Chengdu, China, in 2013 and 2018, respectively.

He is currently a Lecturer with the Guangdong University of Technology, Guangzhou, China. His research interests include the intelligent fault diagnosis and health management for the power drive system, and intelligent control system for multienergy system.

Juntong Liu received the B.E. degree in electrical engineering and automation from the Guangdong University of Technology, Guangzhou, China, in 2022. He is currently working toward the master's degree in electrical engineering with the School of Automation, Guangdong University of Technology, Guangzhou.

His current research interests include fault diagnosis of traction drive systems.

Jinxin Zhang received the Bachelor of Electrical Engineering degree from Foshan University, Foshan, China, in 2024. He is currently working toward the Master of Electrical Engineering degree with the School of Automation, Guangdong University of Technology, Guangzhou, China.

His current research interests include fault diagnosis of traction drive systems.

Haohuan Luo was born in Guangdong, China, in 2001. He is currently working toward the B.S. degree in electrical engineering at Guangdong University of Technology, Guangdong, China.

His research interests include fault diagnosis and health management of traction converter system.

Hanmin Sheng received the B.Sc. and Ph.D. degrees in electrical engineering from Southwest Jiaotong University, Chengdu, China, in 2011 and 2017, respectively.

In 2015, he was a Visiting Scholar with the Nanyang Technological University, Singapore. Since 2017, he has been with the School of Automation, University of Electronic Science and Technology of China, where he is currently an Associate Professor. His research interests include artificial intelligence and detection technology.

Jie Tao received the B.S. degree in automation from the Harbin Institute of Technology, Harbin, China, in 2013 and the Ph.D. degree from the Department of Control Science and Engineering, Zhejiang University, Hangzhou, China, in 2018.

He is currently with the Guangdong Provincial Key Laboratory of Intelligent Decision and Cooperative Control, Guangdong University of Technology, Guangzhou, China. His current research interests include event-based control, networked control systems and unmanned aerial systems.